

Electronic structures of Bi_2Se_3 and $\text{Ag}_x\text{Bi}_2\text{Se}_3$ under pressure studied by high-resolution x-ray absorption spectroscopy and density functional theory calculations

Hitoshi Yamaoka¹, Harald O. Jeschke², Xiaofan Yang², Tong He², Hidenori Goto²,
Nozomu Hiraoka³, Hirofumi Ishii³, Jun'ichiro Mizuki⁴, and Yoshihiro Kubozono²

¹RIKEN SPring-8 Center, Sayo, Hyogo 679-5148, Japan

²Research Institute for Interdisciplinary Science, Okayama University, Okayama 700-8530, Japan

³National Synchrotron Radiation Research Center, Hsinchu 30076, Taiwan, Republic of China

⁴Graduate School of Science and Technology, Kwansai Gakuin University, Sanda, Hyogo 669-1337, Japan



(Received 19 May 2020; revised 9 September 2020; accepted 10 September 2020; published 14 October 2020)

The pressure-induced change in the electronic structures of the superconductors Bi_2Se_3 and $\text{Ag}_x\text{Bi}_2\text{Se}_3$ has been measured with high-resolution x-ray absorption spectroscopy. As a common feature for these compounds, we find that pressure causes the broadening of the Se $4p$ band and an energy shift of the Bi $6s$ band above the Fermi level up to the pressure of the first structural transition. These results, corroborated by density functional theory calculations, correlate with an increase of the carrier density, the disappearance of the band gap, and the emergence of superconductivity. The electronic structure changes significantly at the pressure of the first structural transition, which may be a trigger of the emergence of superconductivity, while above the pressure of the first phase transition it does not change much even around the second phase transition pressure, corresponding to the nearly constant T_c above the pressure of the second structural transition.

DOI: [10.1103/PhysRevB.102.155118](https://doi.org/10.1103/PhysRevB.102.155118)

I. INTRODUCTION

Bi_2Se_3 and Bi_2Te_3 are prototypical examples of three-dimensional (3D) topological insulators [1,2]. Some topological insulators show superconductivity at low temperatures, and chemical doping or pressure also often induces bulk superconductivity, even if the parent material does not show superconductivity [3]. Bi_2Se_3 under pressure is considered a candidate for topological superconductivity [4]; the fact that the upper critical field H_{c2} exceeds both Pauli and orbital limits indicates an unconventional pairing state [5]. The complex evolution of crystal structures under pressure in combination with open questions about the nature of its superconducting phases makes Bi_2Se_3 a very interesting material to study under high pressure [6]. In Bi_2Se_3 , a phase transition from the low-pressure rhombohedral phase (α - Bi_2Se_3) to a monoclinic structure (β - Bi_2Se_3) occurs above 10 GPa [5,7,8]. The emergence of superconductivity was observed around 11–12 GPa with a superconducting transition temperature (T_c) of 4.4 K. T_c increases rapidly to a maximum of 8.2 K at 17.2 GPa, decreases to around 6.5 K at 23 GPa, and then remains almost constant with a further increase in pressure. Variations in T_c with respect to pressure are closely related to the carrier density, which increases by over two orders of magnitude from 2 to 23 GPa. Therefore, the measurement of the electronic structure under pressure may be a key to understanding the mechanism of the emergence of the topological superconductor.

Metal (Cu, Sr, and Ag) doped Bi_2Se_3 also shows superconductivity under pressure [5,9–16]. In $\text{Cu}_x\text{Bi}_2\text{Se}_3$, the copper atoms are intercalated into the weakly bonded Se-Se van der-Waals gaps. Theoretically, a nematic superconductor with

odd parity pairing has been proposed based on Ginzburg-Landau theory [17,18]. On the other hand, scanning tunneling spectroscopy suggested a fully gapped conventional s -wave superconducting pairing symmetry without in-gap states [19]. In contrast, in $\text{Sr}_x\text{Bi}_2\text{Se}_3$ most of the doped Sr atoms are located in the Se-Bi-Se-Bi-Se quintuple layer [9,20]. The Sr doping moves the Fermi level upward, resulting in an increase of the carrier density [20]. $\text{Sr}_x\text{Bi}_2\text{Se}_3$ exhibits superconductivity with high superconducting volume fraction [16]. Another property of $\text{Sr}_x\text{Bi}_2\text{Se}_3$ is that the topological surface state is well separated from the bulk bands [16,20,21]. Furthermore, a pressure-induced second superconducting phase emerges above 6 GPa in $\text{Sr}_{0.065}\text{Bi}_2\text{Se}_3$, with a maximum T_c value of 8.3 K [15]. The reemergence of superconductivity in $\text{Sr}_{0.065}\text{Bi}_2\text{Se}_3$ may correlate to the structural phase transition from an ambient pressure rhombohedral phase to a high-pressure monoclinic phase around 6 GPa, and further to another high-pressure tetragonal phase above 25 GPa. However, the latter structural transition around 25 GPa did not effect changes in T_c . A similar pressure-induced emergence of superconductivity was also found in $\text{Ag}_x\text{Bi}_{2-x}\text{Se}_3$ [9]. In $\text{Ag}_x\text{Bi}_{2-x}\text{Se}_3$, structural phase transitions occur at 8 and 23 GPa and two kinds of superconductivity (low- T_c phase at 10–24 GPa and high- T_c phase at 17–26 GPa) were found, where the high- T_c phase extended above 24 GPa across the phases II and III. It has been suggested that a filamentary phase III was formed above 17 GPa before the emergence of the bulk phase III above 23 GPa. It was pointed out that Ag doping possibly tunes the Fermi level downward [9]. Ag-substituted and Sr-intercalated systems were claimed to be spin-triplet p -wave superconductors [5,9,15]. $\text{A}_x\text{Bi}_{2-x}\text{Se}_3$

($A = \text{Sr, Ag}$) may be ideal systems to study topological superconductivity under pressure.

The emergence of the superconductivity and the increase of T_c under pressure in these compounds may also correlate to the change in the electronic structure. However, the electronic structure under pressure has so far been studied neither for the parent material of Bi_2Se_3 nor for metal-doped Bi_2Se_3 . Thus, Bi_2Se_3 and $A_x\text{Bi}_{2-x}\text{Se}_3$ can be considered good examples to study the origin of superconductivity under pressure systematically. In this paper, we report a detailed study of the electronic structures of Bi_2Se_3 and $\text{Ag}_{0.05}\text{Bi}_{1.95}\text{Se}_3$ under pressure. The purpose of this paper is to clarify the correlation of the electronic structure to crystal structure and superconductivity under pressure. We measured the pressure dependence of the x-ray absorption spectra in partial fluorescence yield mode (PFY-XAS), which gives high-resolution spectra, at the Se- K and Bi- L_3 absorption edges [22–24]. We measured the electronic structures of the two key elements of Bi and Se separately. It is noted that our XAS study is intrinsically bulk sensitive and thus cannot discuss the surface states or surface topology, while here we study the correlation between bulk electronic structure and superconductivity. Pressure is expected to tune the electronic structure such as the density of states (DOS) at the Fermi level especially near the pressure where superconductivity emerges. We also performed density functional theory (DFT) calculations of Bi_2Se_3 with fully relativistic GGA+SO. The DFT calculations show that the DOS at the Fermi level appears above the pressure of the first structural transition and rapidly increases with pressure, which is a prerequisite for the emergence of superconductivity.

II. METHODS

A. Experiments

Single crystals of Bi_2Se_3 , $\text{Ag}_{0.05}\text{Bi}_{1.95}\text{Se}_3$, $\text{Sr}_{0.54(7)}\text{Bi}_2\text{Se}_{4.2(1)}$, and $\text{Sr}_{0.09(3)}\text{Bi}_2\text{Se}_{3.61(4)}$ were prepared with SeO_2 , Bi, and Bi_2O_3 for comparison [9]. Crystals of Bi_2Se_3 and metal-doped Bi_2Se_3 were grown by a conventional melt-growth method using stoichiometric amounts of Ag, Sr, Bi, and Se powders [9]. The analyses of chemical composition were performed by an energy-dispersive x-ray (EDX) spectrometer equipped with a scanning electron microscope (KEYENCE VE-9800-EDAX Genesis XM2). The EDX spectra were measured for five different positions of the metal-doped lumps at room temperature. In the case of a small amount of Ag doping, Ag is substituted on the Bi site [9]. On the other hand, Sr can be doped into Se-Bi-Se-Bi-Se quintuple layers or inserted between Bi and inner Se layers [9,20,25].

Measurements of the PFY-XAS spectra were performed at BL12XU, SPring-8 [26,27]. At the BL12XU beamline of SPring-8, the undulator beam was monochromatized by a cryogenically cooled double crystal Si(111) monochromator. We measured the PFY-XAS spectra at the Se- K and Bi- L_3 absorption edges. This are essentially bulk-sensitive measurements and we measure the bulk electronic structures. Johann-type spectrometers were equipped with a spherically bent Si(577) analyzer of radius of ~ 1 m for Se $K\beta_1$ and Si(555) for Bi $L\alpha_1$ emissions from the samples. A Si

solid-state detector (Amptech) was used to analyze the $K\beta$ emission of the $3p_{3/2} \rightarrow 1s$ deexcitation at the Se- K absorption edge and the $L\alpha$ emission of the $3d_{5/2} \rightarrow 2p_{3/2}$ deexcitation at the Bi- L_3 absorption edge. We used the $K\beta$ emission of Se to measure the PFY-XAS spectra, instead of using the $K\alpha$ emission [28], because the Se $3p$ electrons may be more correlated to the outer shell electrons compared to the $2p$ electrons. At the emitted photon energy of 12.66 keV, the overall energy resolution was set to be 1.5 eV. Note that one can discuss relative changes in energy on the order of 0.1 eV, which is one order of magnitude smaller than the energy spread of the measurement system. The intensities of the measured spectra were normalized using the intensity of the incident beam that was monitored just before the sample. The errors of the intensity and energy of each component of the PFY-XAS spectrum originate mainly from the statistical errors of the total counts and the fit errors. The intensities of the PFY-XAS spectra are normalized by the areas in the measured-energy range.

For the high-pressure experiments in the x-ray emission spectroscopy, the x-ray beam was focused to 30 (horizontal) \times 14 – 20 (vertical) μm^2 at the sample position using a toroidal and a Kirkpatrick-Baez mirror. High-pressure conditions were achieved using a diamond anvil cell (DAC) coupled with a gas-membrane. A Be-gasket 3 mm in diameter and approximately 100 μm thick was preindented to approximately 40 μm thickness around the center. The diameter of the sample chamber in the gasket was approximately 120 μm , and the diamond anvil culet size was 300 μm . A pressure medium of Daphne 7474 was used for the DAC. Pressure was monitored by the ruby fluorescence method [29–31]. All measurements were performed at room temperature. We note that no structural transition has been reported for Bi_2Se_3 in the temperature range 10–270 K [32].

B. Theoretical calculations

We performed scalar relativistic electronic structure calculations for Bi_2Se_3 with the full potential local orbital (FPLO) basis set [33] and the GGA exchange correlation functional [34]. The calculations for the doped Bi_2Se_3 systems have not been performed because it is necessary for the DFT calculations to know exactly where a dopant sits in the crystal, and the dopant positions of Ag and Sr are still under discussion [25,35,36]. We use $24 \times 24 \times 24$ k meshes at $P = 0, 4.8,$ and 37.8 GPa and a $12 \times 12 \times 12$ k mesh at $P = 13.5$ GPa. The evolution of the structure of Bi_2Se_3 with pressure has been investigated repeatedly [8,37,38], with some differences in transition pressures and high-pressure crystal structures. The ambient pressure hexagonal space group $R\bar{3}m$ is replaced at around 10 GPa by a monoclinic $C2/m$ space group. At pressures above about 25 GPa, there is either another monoclinic or a tetragonal $I4/mmm$ space group [8]. We use the ambient pressure and $P = 13.5$ GPa structures of Ref. [37], and the $P = 4.8$ and 37.8 GPa structures of Ref. [38]. For investigating the continuous evolution of quantities as a function of pressure, we use a smooth evolution of lattice parameters from Ref. [39], combined with DFT relaxation of internal Bi and Se coordinates. We investigate the effects of spin-orbit (SO) coupling using fully relativistic GGA calculations (to which we refer as GGA+SO).

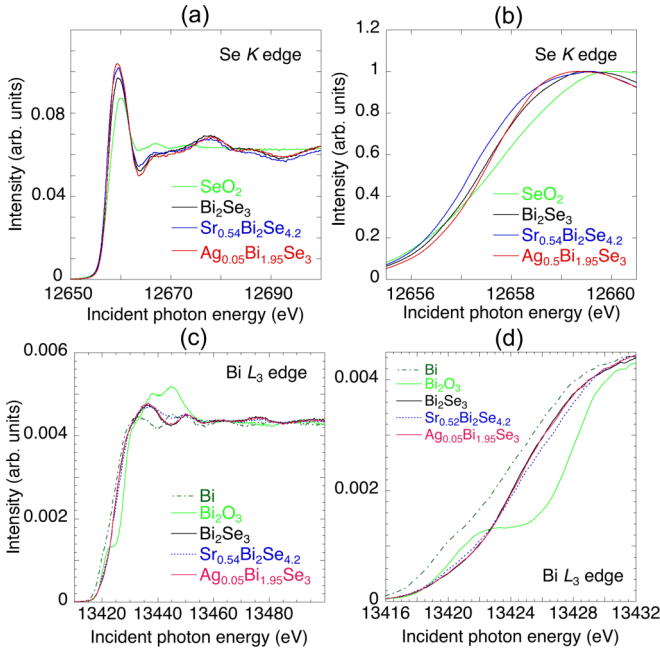


FIG. 1. (a) PFY-XAS spectra of SeO_2 , Bi_2Se_3 , $\text{Sr}_{0.54}\text{Bi}_2\text{Se}_{4.2}$, and $\text{Ag}_{0.05}\text{Bi}_{1.95}\text{Se}_3$ at the Se- K absorption edge. The intensity is normalized by the area. (b) Expanded views of the PFY-XAS spectra in (a) around the Se- K absorption edge. The intensity is normalized by the peak intensity. (c) PFY-XAS spectra of Bi, Bi_2O_3 , Bi_2Se_3 , $\text{Sr}_{0.54}\text{Bi}_2\text{Se}_{4.2}$, and $\text{Ag}_{0.05}\text{Bi}_{1.95}\text{Se}_3$ at the Bi- L_3 absorption edge. (d) Expanded views of the PFY-XAS spectra in (c) around the Bi- L_3 absorption edge.

III. RESULTS AND DISCUSSION

A. Chemical composition dependence

Figure 1(a) shows PFY-XAS spectra of SeO_2 , Bi_2Se_3 , $\text{Sr}_{0.54}\text{Bi}_2\text{Se}_{4.2}$, and $\text{Ag}_{0.05}\text{Bi}_{1.95}\text{Se}_3$ at the Se- K absorption edge and at ambient pressure. Oxidation numbers of Se of the Bi_2Se_3 -based samples are smaller than that of SeO_2 . The Se- K absorption edge of the Sr-doped samples shifts to lower energy compared to that of Bi_2Se_3 , while that of the Ag-doped samples shifts to slightly higher energy. A small amount of Ag doping leads to hole doping in the case of Ag substitution to the Bi site because the change in the cations from Bi^{3+} to Ag^+ adds two holes to the system [9,11]. Very recently the occurrence of both possibilities—the intercalation of Ag and the substitution of Ag to the Bi site—were observed [35,36]. It is expected that with increasing Ag doping, the fraction of intercalated Ag increases, keeping the Fermi level at the bottom of the conduction band. On the other hand, doped Sr is expected to be intercalated into the van-der-Waals gap between Se-Se layers, providing one electron per Sr atom to the system. However, it was reported that Sr atoms are possibly inserted between Bi and inner Se layers [25,40]. The present results indicate hole doping in $\text{Ag}_{0.05}\text{Bi}_{1.95}\text{Se}_3$ and electron doping in $\text{Sr}_{0.54}\text{Bi}_2\text{Se}_{4.2}$.

Figure 1(c) shows PFY-XAS spectra of Bi, Bi_2O_3 , Bi_2Se_3 , $\text{Sr}_{0.54}\text{Bi}_2\text{Se}_{4.2}$, and $\text{Ag}_{0.05}\text{Bi}_{1.95}\text{Se}_3$ at the Bi L_3 -absorption edge. The oxidation numbers of Bi for Bi_2Se_3 , $\text{Sr}_{0.54}\text{Bi}_2\text{Se}_{4.2}$, and $\text{Ag}_{0.05}\text{Bi}_{1.95}\text{Se}_3$ are higher than those for Bi_2O_3 and Bi if we define the Bi L_3 absorption edge for the shoulder peak of

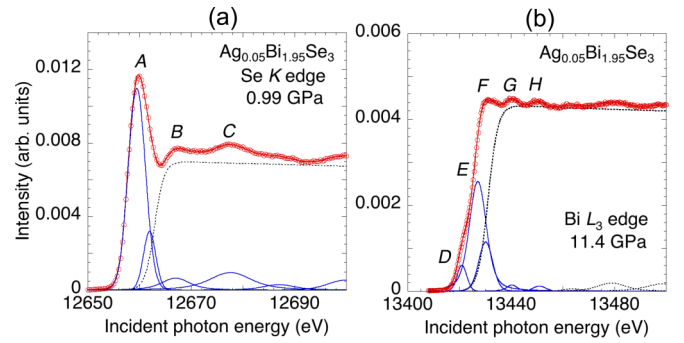


FIG. 2. (a) A fit example of the PFY-XAS spectra of $\text{Ag}_{0.05}\text{Bi}_{1.95}\text{Se}_3$ at the Se- K absorption edge and at 0.99 GPa. Main peaks around the absorption edge are labeled as A, B, and C. (b) A fit example of the PFY-XAS spectra of $\text{Ag}_{0.05}\text{Bi}_{1.95}\text{Se}_3$ at the Bi- L_3 absorption edge and at 11.4 GPa. Main peaks around the absorption edge are labeled as D, E, F, G, and H.

Bi_2O_3 . The spectrum of $\text{Ag}_{0.05}\text{Bi}_{1.95}\text{Se}_3$ is very similar to that of Bi_2Se_3 at the Bi- L_3 absorption edge. On the other hand, the Sr doping causes a small shift of the weak peak around 13422 eV to lower incident energy as shown in Fig. 1(d). The Ag doping to Bi_2Se_3 is less effective compared to the case of the Sr doping on the change in the electronic structure of the Bi site at ambient pressure. A small peak at 13 422 eV of Bi_2O_3 is much stronger than those of other samples, revealing a larger 6s unoccupied band of the Bi site of Bi_2O_3 [41,42]. The present results agree with the DFT calculations by Deng *et al.* [43] that the band gap and Bi s DOS above the Fermi level of Bi_2O_3 is larger compared to Bi_2Se_3 , and the density of states (DOS) above the Fermi level of Bi_2O_3 shows a step-like increase.

B. Analyses of the PFY-XAS spectra

The absorption spectra reflect the DOS of the vacant shells (electron-empty states) above the Fermi level. Pressure normally induces a broadening of the DOS and a shift of the Fermi level. It is also expected that the pressure-induced shift of the energy of the DOS or that of the absorption edge may correlate to the shift of the Fermi level or the change in DOS at the Fermi level. The partial DOS of Se 4p and Bi 6p contributes mostly to the total DOS near the Fermi level as described in the subsection on theoretical calculations (Sec. II B). Spectroscopically, however, we observe mainly the dipole-allowed transitions of Se 1s-4p, Bi 2p-6s, and Bi 2p-6d, and the observed spectra do not reflect the Bi 6p DOS. We fitted the spectra to see the detailed change in DOS under pressure. In Fig. 2, we show examples of the fits to the PFY-XAS spectra at the Se- K and Bi- L_3 absorption edges [44]. We assumed some Voigt functions with an arctan-like background function for simplicity. For the peak A, two symmetric components are assumed because of an asymmetric profile. From the analogy to the spectra of selenium compounds at the Se- K absorption edge [45–49], the peak A is attributed to a 1s-4p dipole transition and Se 4d partial density of states hybridized with the Bi 6s and 6p states. The peak B is due to multiple scattering sensitive to the local structure around Se and the partial density of states of Se 4d character in the continuum.

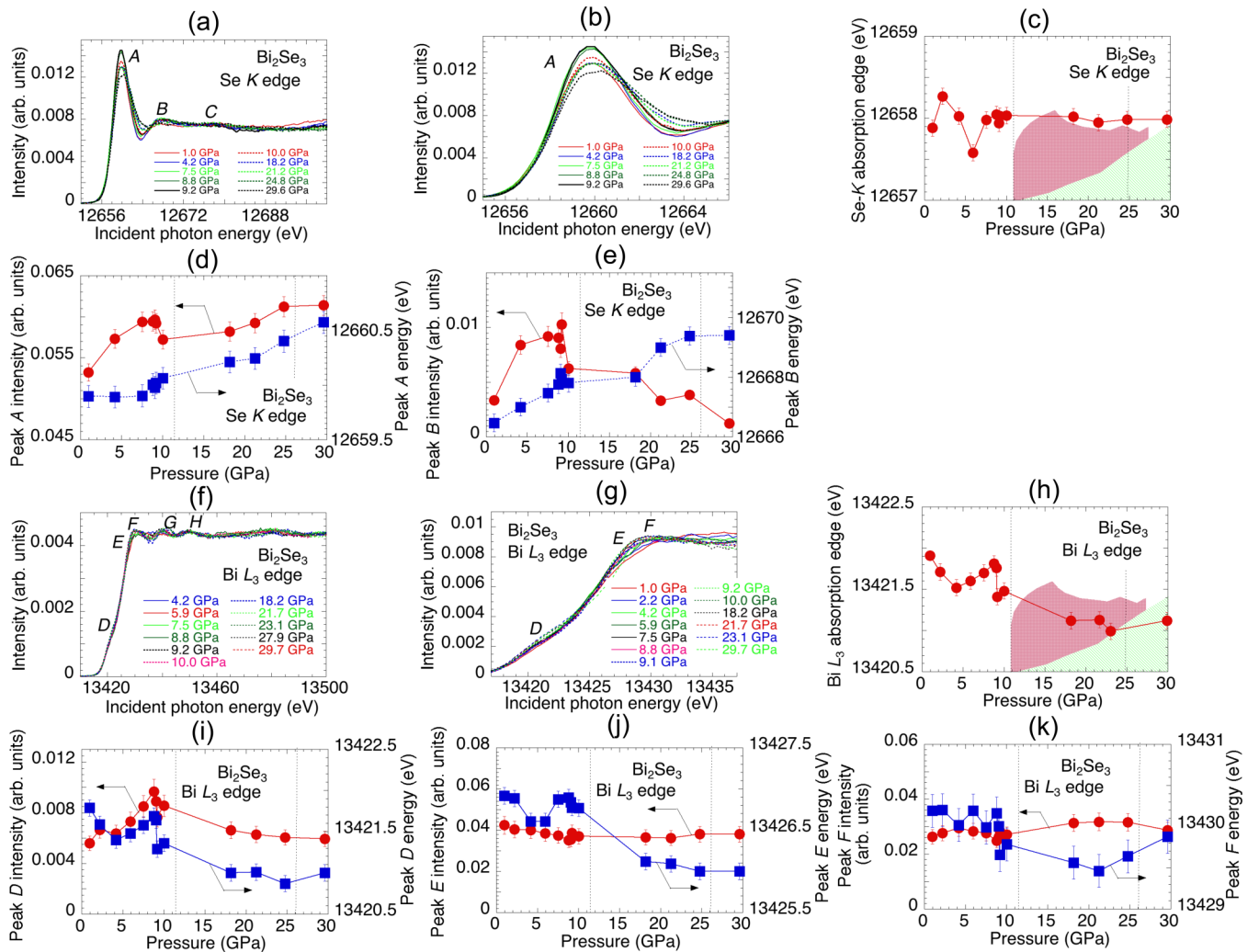


FIG. 3. (a) Pressure dependence of the PFY-XAS spectra of Bi_2Se_3 at the Se- K absorption edge. (b) Expanded views of the PFY-XAS spectra in (a) around the Se K -absorption edge. (c) Pressure dependence of the energy of the Se- K absorption edge. (d),(e) Pressure dependence of the intensity and energy of the peaks A and B of the PFY-XAS spectra at the Se- K absorption edge, respectively. (f) Pressure dependence of the PFY-XAS spectra of Bi_2Se_3 at the Bi- L_3 absorption edge. (g) Expanded views of the PFY-XAS spectra in (f) around the Se- K absorption edge. (h) Pressure dependence of the energy of the Bi- L_3 absorption edge. (i),(j),(k) Pressure dependence of the intensity and energy of the peaks D , E , and F of the PFY-XAS spectra at the Bi- L_3 absorption edge, respectively. Pink-colored and green-shaded areas in (c) and (h) correspond to the superconducting regions reported by Kong *et al.* [7] and Kirshenbaum *et al.* [5], respectively, where the maximum value of the vertical axis scales to be 15 K. Vertical dotted lines and yellow area in (c), (d), (e), (h), (i), (j), and (k) correspond to the pressures of the structural transitions [8].

The peak B also possibly arises from the e_g antibonding orbital at the Se site [45].

We assumed some components of the peaks near the Bi- L_3 absorption edge as shown in Fig. 2(b) [41,42,50]. The weak shoulder peak D is assigned as a dipole-allowed transition of a $2p_{3/2}$ electron into $6s$ states [42,49,51,52]. The increase of the intensity of the peak D corresponds to an increase of the holes in the Bi $6s$ states, a lowering of the band filling, and a decrease in the carrier numbers. The peaks E and F correspond to the transition of a $2p_{3/2}$ electron into $6d$ states of t_{2g} (E : nonbonding, d_{xy} and d_{yz}) and e_g (F : antibonding, d_{z^2}) [49]. Thus, the intensity of the peak D reflects the Bi s DOS and those of the peaks E and F correspond to the Bi d DOS above the Fermi level. Note that the ligand-field splitting of d -orbitals into t_{2g} and e_g states occurs. The relative intensities

of the peak D give the relative occupation probabilities of the Bi $6s$ band in the ground state under the assumption that there is no hybridization between the Bi $6s$ and $6d$ orbitals [41]. A pressure-induced shift of the Fermi level may cause a shift of the energy of the peak D (Bi $6s$ DOS) or the energy of the absorption edge. In Figs. 1(c) and 1(d), the PFY-XAS spectrum of Bi_2O_3 shows a weak intensity of the peak D , suggesting that the Bi $6s$ state is not completely filled by electrons [50].

C. Pressure dependence of the PFY-XAS spectra of Bi_2Se_3

We measured the pressure dependence of the PFY-XAS spectra of the parent compound of Bi_2Se_3 as shown in Figs. 3(a) and 3(f) at the Se- K and Bi- L_3 absorption edges.

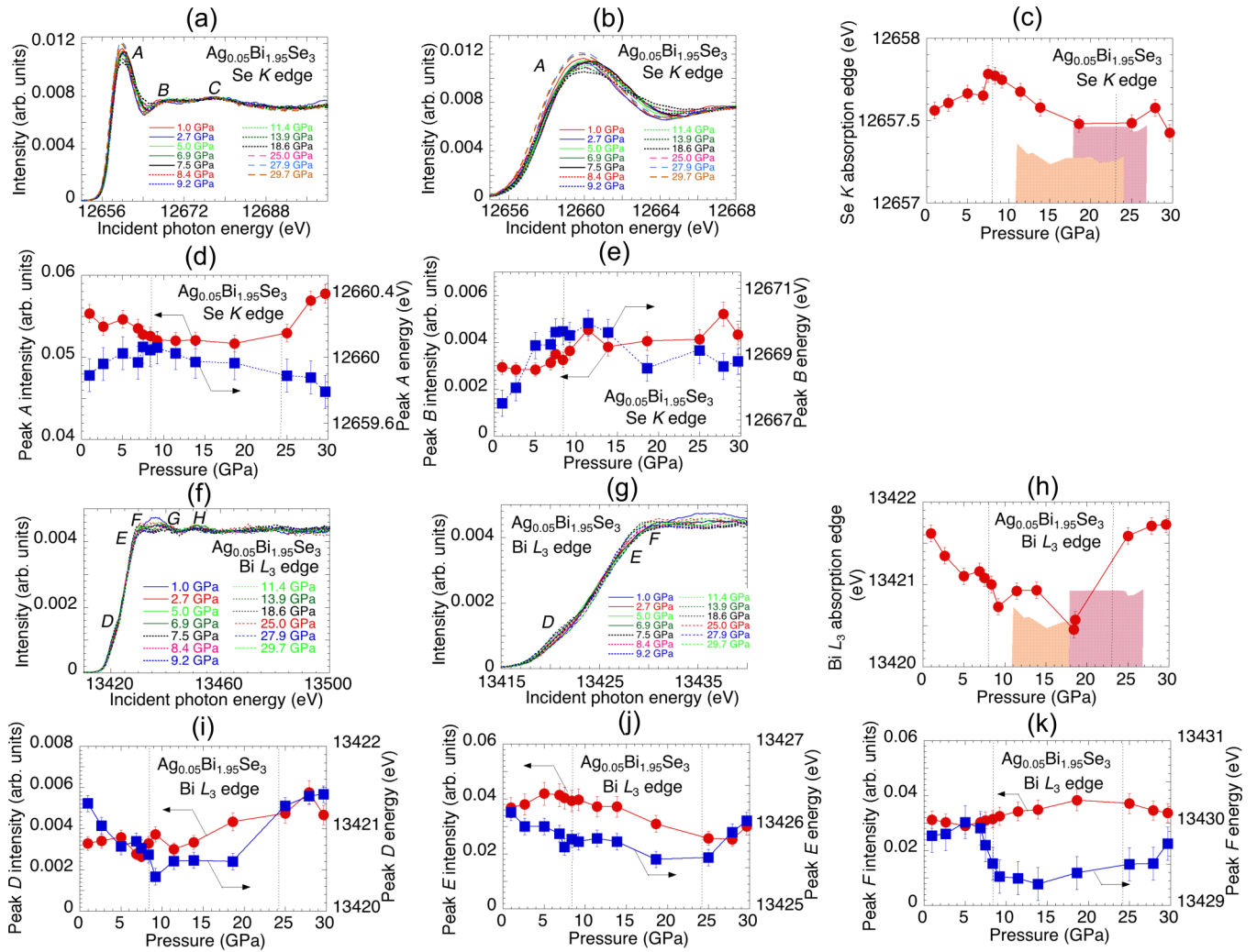


FIG. 4. (a) Pressure dependence of the PFY-XAS spectra of $\text{Ag}_{0.05}\text{Bi}_{1.95}\text{Se}_3$ at the Se-K absorption edge. (b) Expanded views of the PFY-XAS spectra in (a) around the Se-K absorption edge. (c) Pressure dependence of the energy of the Se-K absorption edge. (d),(e) Pressure dependence of the intensity and energy of the peaks A and B of the PFY-XAS spectra at the Se-K absorption edge, respectively. (f) Pressure dependence of the PFY-XAS spectra of $\text{Ag}_{0.05}\text{Bi}_{1.95}\text{Se}_3$ at the Bi-L₃ absorption edge. (g) Expanded views of the PFY-XAS spectra in (f) around the Se K-absorption edge. (g) Pressure dependence of the intensity of the peaks D, E, and F of the PFY-XAS spectra at the Bi-L₃ absorption edge. (i),(j),(k) Pressure dependence of the intensity and energy of the peak D, E, and F of the PFY-XAS spectra at the Bi-L₃ absorption edge, respectively. Colored areas in (c) and (h) correspond to the superconducting regions, where the maximum value of the vertical axis scales to be 15 K [9]. Vertical dotted lines in (c), (d), (e), (h), (i), (j), and (k) correspond to the pressures of the structural transitions [9].

In Bi_2Se_3 , the first and second structural transitions have been reported to occur from $R\bar{3}m$ (rhombohedral, phase I) to $C2/m$ (monoclinic, phase II) at 10–12 GPa and from $C2/m$ to $I4/mmm$ (tetragonal, phase III) at 25–26 GPa, respectively. The width of the peak A in Fig. 3(b) increases with pressure, indicating the broadening of the Se 4*p* band above the Fermi level. The broadening occurs mainly at higher incident energy. A similar pressure-induced feature is also observed in the doped Bi_2Se_3 as shown below. The energy of the Se-K absorption edge is insensitive to pressure, especially at high pressures where superconductivity is observed, as shown in Fig. 3(c). The intensities and energy of the peaks A (Se 4*p* band) and B (Se 4*d* band) at the Se-K absorption edge in Figs. 3(d) and 3(e) show a sudden change around 8–9 GPa below the first phase transition pressure of 10–12 GPa. A possibility to explain this phenomenon is that a filamentary

phase II starts at 8–9 GPa and the electronic structure is sensitive to the transition to phase II. It is noted that in a small amount of Ag-doped sample, $\text{Ag}_{0.05}\text{Bi}_{1.95}\text{Se}_3$, the pressure of the first phase transition was 8.8 GPa [9]. Therefore, it is likely that the present Bi_2Se_3 sample may have the first structural phase transition around 8–9 GPa. Figure 3(h) shows a sudden decrease of the energy of the Bi-L₃ absorption edge at 9 GPa, and the edge energy has a decreasing trend at high pressures. The intensities of the peaks D (Bi 6*s* band), E (Bi *t*_{2*g*} band), and F (Bi *e*_g band) at the Bi-L₃ absorption edge also show a change around 8–9 GPa as shown in Figs. 3(i), 3(j), and 3(k), respectively.

In Bi_2Se_3 , the carrier density increases on a logarithmic scale up to 47 GPa, shows a sudden increase at 11 GPa, and superconductivity emerges above 11 GPa [5,7]. The superconducting transition temperature (*T*_c) correlates with the increase

of the carrier density up to 28 GPa in the measurements by Kirshenbaum *et al.* [5], while T_c in the measurements by Kong *et al.* [7] increased suddenly above 11 GPa, as shown in Fig. 3(c). But T_c does not change much with a further increase of pressure in both measurements. The increase of the intensity of the peak D up to 8 GPa corresponds to the increase of the holes of the Bi $6s$ state and the decrease of the electron carrier density if we assume that there is no hybridization between the Bi $6s$ and $6d$ orbitals. This is inconsistent with the results of the increase of the carrier density obtained from the Hall coefficient measurement [5,7]. Here, two possibilities could be considered to explain this inconsistency: one is the increase of the hybridization of the Bi $6s$ states and another is the increase of holes as carriers. The latter case is refuted by the Hall coefficient measurement because the carriers are electrons [5] and thus the pressure-induced increase of the hybridization is more likely. The decrease of the intensity of the peak D above 8 GPa may be caused by the increase of the carrier density which is filling the Bi $6s$ states. The electronic structures of both Se and Bi changed around the first phase transition pressure as described above, while the change in the electronic structure at the second structural transition pressure of 26 GPa was not observed clearly. Here, we note that the carrier density was derived in Ref. [5] assuming a single band model, but the actual band structure is very complex as described below. Furthermore, the signal intensity of the Hall-coefficient measurement is proportional to the inverse of the carrier density and it was normally very weak in the metallic phase, and thus the measurement may be unreliable especially at high pressures.

Our high-resolution measurements show a clear shoulder component of the peak D (Bi $6s$ band) around the Bi L_3 absorption edge. The present results agree with the DFT calculations shown below; the intensity of the peak D , i.e., the Bi s DOS, increased gradually up to 10 GPa and the energy of the peak D slightly increased above 5 GPa as shown in Fig. 3(i). Thus, the energy shift of the peak D may reflect the shift of the Fermi level or the change in the DOS at the Fermi level. The other remarkable result is that the energies of the peaks D , E , and F shift to lower incident energy after the first structural transition as shown in Figs. 3(i), 3(j), and 3(k).

These results may suggest that pressure causes an upward shift of the Fermi level or an increase of the DOS at the Fermi level after the first structural transition, resulting in the disappearance of the band gap at high pressures, and the increase of the carrier density above the Fermi level, correlating to the emergence of superconductivity. The first structural phase transition is a trigger of the emergence of the superconductivity, with significant changes of the crystal structure as well as the electronic structure, and above the pressure of the first phase transition the electronic structure does not change much, which correlates to nearly constant T_c . This scenario seems to be shared by the doped Bi_2Se_3 superconductors described below, although a shift of the phase transition pressure occurs. A correlation between carrier density and superconductivity is also observed in the topological superconductors Sb_2Se_3 [53], the telluride compounds of Sn-doped $\text{Bi}_{1.1}\text{Sb}_{0.9}\text{Te}_2\text{S}$ [54], BiTeI [55], $\text{Bi}_{1.5}\text{Sb}_{0.5}\text{Se}_{1.3}\text{Te}_{1.7}$ [56], Sb_2Te_3 [57], and bismuth telluride-based alloys [58]. The closing of the band gap, the increase of the carrier

density, and the emergence of superconductivity with pressure, resulting in the disappearance of the insulating nature, are correlated with each other. The DOS at the Fermi level has an important impact on superconductivity. We note that the increase of the carrier density with pressure up to the first structural transition pressure may correlate to the increase of the DOS at the Fermi level.

In Bi_2Se_3 , a pressure-induced electronic topological transition (ETT) in the $R\bar{3}m$ phase was suggested at ~ 3 GPa from the pressure dependence of the c/a ratio [8], at 3–5 GPa from XRD [37], at 5 GPa from Raman scattering [37], and at 6.5 GPa from the carrier density jump in the Hall coefficient measurement [37]. Bera *et al.* termed the transition at 2.4 GPa from the Raman spectroscopy as an isostructural transition instead of ETT [59]. First-principles calculations also showed that the low-pressure transition around 3 GPa was not related to a change in the electronic topology [59]. Our results show that the energies of the Bi absorption edge, the peak D , and the peak E go through a minimum around 4–5 GPa as shown in Figs. 3(h), 3(i), and 3(j), respectively. These changes in the Bi electronic structure possibly correlate to the pressure-induced electronic topological transition in the $R\bar{3}m$ phase, while the DFT calculations show no change in the density of states at the Fermi level around this pressure range (see Fig. 8 below).

D. Pressure dependence of the PFY-XAS spectra of $\text{Ag}_{0.05}\text{Bi}_{1.95}\text{Se}_3$

Figures 4(a) and 4(f) show the pressure dependence of the PFY-XAS spectra of $\text{Ag}_{0.05}\text{Bi}_{1.95}\text{Se}_3$ at the Se- K and Bi- L_3 absorption edges. The width of the peak A in Fig. 4(b) increases with pressure, and a broadening of the Se $4p$ band above the Fermi level occurs. The pressure-induced behavior of the energy of the Se- K absorption edge in $\text{Ag}_{0.05}\text{Bi}_{1.95}\text{Se}_3$ is different from that in Bi_2Se_3 . The energy of the Se- K absorption edge in Fig. 4(c) increases slightly with pressure up to 8 GPa, shows a sudden increase around the pressure 8 GPa of the first structural transition, and decreases gradually up to 19 GPa. The intensity of the peak A in Fig. 4(d) decreases slightly with pressure up to 20 GPa and increases above the pressure of the second structural transition, while its energy does not change much. The intensity and energy of the peak B in Fig. 4(e) increase gradually up to around 10 GPa.

The energy of the Bi- L_3 absorption edge in Fig. 4(h) decreases with pressure up to 9 GPa, shows a rapid transition around 8 GPa, and returns to the original energy at ambient pressure above the second structural transition. A similar trend is observed in the pressure dependence of the energy of the peak D in Fig. 4(i). An apparent change in the energy of the peak F in Fig. 4(k) is observed around the pressure of the first structural transition, while the pressure dependence of the peak F is small. The intensities of the peaks D , E , and F in Figs. 4(i), 4(j), and 4(k) do not show a clear change at the pressures of the structural transitions. The intensities of the peaks D show a different behavior under pressure compared to the case of Bi_2Se_3 . In $\text{Ag}_{0.05}\text{Bi}_{1.95}\text{Se}_3$, it does not change up to around 8 GPa although it becomes unstable at this pressure, and it increases gradually with further increase of the pressure as shown in Fig. 4(i). The Ag substitution corresponds to hole doping [9,35], but the Hall-coefficient measurement

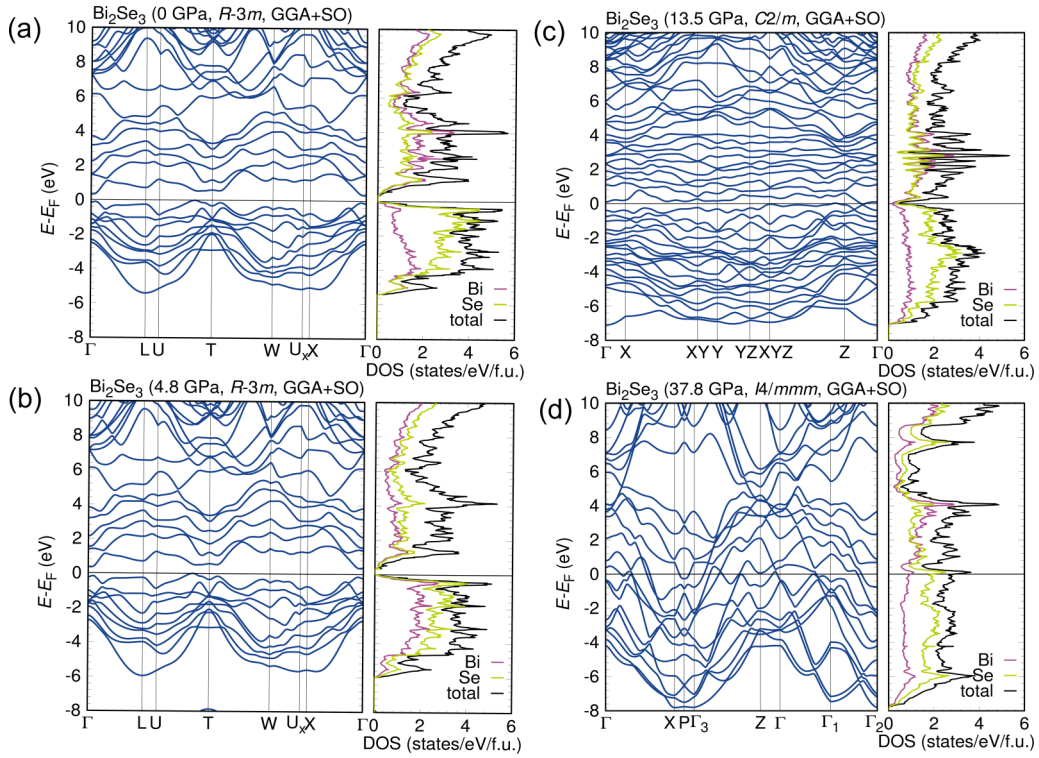


FIG. 5. Band structure and density of states (DOS) of Bi_2Se_3 (a) at $P = 0$ GPa, (b) $P = 4.8$ GPa, (c) $P = 13.5$ GPa, and (d) $P = 37$ GPa. Structures for (a) and (c) are taken from Ref. [37], those for (b) and (d) from Ref. [38].

showed that the carriers are still electrons [11]. The Ag doping changes the Fermi level downward [9,11]. On the other hand, the pressure decreases the energy of the peak D , suggesting an upward change in the Fermi level. The results for Bi_2Se_3 indicate that pressure increases the hybridization and the number of holes in the Bi $6s$ band as revealed by the increasing intensity of the peak D . In $\text{Ag}_{0.05}\text{Bi}_{1.95}\text{Se}_3$, these two pressure-induced effects may compete with each other and result in the nearly constant intensity of the peak D below 8 GPa.

The energy shift of the peak D up to 10 GPa from ambient pressure is large, of the order of 1 eV, and may correspond to the raising of the Fermi level or to a change in the DOS at the Fermi level, and then the system may undergo the transition from an insulator with an indirect gap to metal as calculated for Bi_2Se_3 [60,61]. Both the energies of the peak D and the absorption edge return to higher incident energy above the pressure of the second structural transition, but the metallic character may be kept because the Se $4d$ DOS (the peak A intensity) still shifts to lower incident energy with pressure, as shown in Fig. 4(c).

The difference of the behavior of the superconductivity among Bi_2Se_3 , $\text{Cu}_x\text{Bi}_2\text{Se}_3$, and $\text{Sr}_x\text{Bi}_{2-x}\text{Se}_3$ has been explained qualitatively with a simple theoretical BCS model of a low carrier density superconductor, where $T_c \sim \Theta_D \exp\{-1/[N(0)V_0]\}$ [Θ_D : Debye temperature, $N(0) \sim m^*n^{1/3}$: the density of states with effective mass m^* at the Fermi level, and V_0 : the effective electron-phonon interaction parameter] [5,12,14,15]. In Bi_2Se_3 , the carrier density increased with pressure [5]. In $\text{Cu}_x\text{Bi}_2\text{Se}_3$, n decreased with pressure [12]. In $\text{Sr}_{0.065}\text{Bi}_{2-x}\text{Se}_3$, the reduction of the charge

carrier density occurred under pressure and the DOS at the Fermi level decreased at low pressures [14,15]. It has been considered that these differences may cause the different pressure dependence of T_c . In $\text{Sr}_{0.065}\text{Bi}_2\text{Se}_3$, a steplike increase of the superconductivity above the pressure of the first phase transition was observed [15]. In $\text{Nb}_x\text{Bi}_2\text{Se}_3$, T_c showed a different behavior from Cu- and Sr-substituted systems; T_c increased with pressure at low pressures [62]. Additional Fermi surface features of the Nb-substituted system have been suggested as an explanation.

In Bi_2Se_3 the electronic structures of both Bi and Se change significantly at the phase transition from I to II, while they seem to be not sensitive at the transition from II to III as shown in Fig. 3. In $\text{Ag}_{0.05}\text{Bi}_{1.95}\text{Se}_3$ they show a similar trend to the case of Bi_2Se_3 , but the changes in the intensity and energy of the peaks A , B , and E are not clearly observed at the phase transition from I to II as shown in Figs. 4(d), 4(e), and 4(j), respectively.

Recently, a similar pressure-induced behavior of T_c was found in $\text{Bi}_2\text{Te}_2\text{Se}$ and $\text{Bi}_{1.1}\text{Sb}_{0.9}\text{Te}_2\text{S}$, and a universal phase diagram was proposed combining the results of Bi_2Se_3 , Bi_2Te_3 , and $(\text{Bi,Sb})_2(\text{Se,Te})_3$, where the superconducting regions were divided into low- T_c SC1 and high- T_c SC2 as a function of pressure [60]. In the universal phase diagram, the transition from SC1 to SC2 occurred around the pressure of the structural phase transition from monoclinic ($C2/m$) to tetragonal ($I4/mmm$) phases. Meanwhile, in $\text{Sr}_{0.065}\text{Bi}_2\text{Se}_3$ the sudden increase of T_c occurred at the end of the $R\bar{3}m$ phase around the pressure of the phase transition from $R\bar{3}m$ to $C2/m$, where both phases of $R\bar{3}m$ and $C2/m$ coexisted from the pressure at which low T_c superconductivity appeared up

to the end of the $R\bar{3}m$ phase. However, this universal phase diagram cannot be applied to the steplike increase of T_c in $\text{Sr}_{0.065}\text{Bi}_2\text{Se}_3$.

In the Bi oxide superconductor $\text{Ba}_{1-x}\text{K}_x\text{BiO}_3$, the intensity of the peak D and the Bi valence were a measure of the superconductivity [41]. Upon increasing potassium content, the volume and T_c decreased, and the intensity of the peak D increased with increasing Bi valence. In $\text{Ba}_{1-x}\text{K}_x\text{BiO}_3$, the Bi valence was considered to be between 4+ and 5+. In Bi_2Se_3 and $\text{Ag}_{0.05}\text{Bi}_{1.95}\text{Se}_3$, the intensity of the peak D shows a sudden change around the pressure 8 GPa of the first structural transition. Figure 1(d) shows that the Bi valences of the Bi_2Se_3 -based compounds are slightly larger than 3+. The present Bi_2Se_3 -based samples do not show a correlation between the intensity of the peak D and the Bi valence.

Additionally, we also measured the pressure dependence of the electronic structure of $\text{Sr}_x\text{Bi}_2\text{Se}_3$ and Bi [44]. In $\text{Sr}_x\text{Bi}_2\text{Se}_3$, T_c showed interesting behavior as a function of pressure as described above [10,14–16,25,63]. The results possibly suggest the closing of the band gap and correlate with the increase of T_c above 11 GPa, although the superconductivity of the highly doped samples remains an unresolved problem. Bi is known to have five phases up to 15 GPa [64–70]. In Bi, a change in the electronic structure around the pressure 7 GPa of the phase transition from phase III to V was observed, while the change from phase II to III, where superconductivity emerges, was small.

E. Electronic structure calculations of Bi_2Se_3

The band structure and DOS of Bi_2Se_3 calculated with fully relativistic GGA+SO (spin orbit) are shown in Fig. 5. A Dirac cone is situated at the Γ point. Comparison of the GGA+SO calculations with GGA shows that spin-orbit coupling opens a gap in the symmetry-protected Dirac cone [44]. A band gap is observed at 0 and 4.8 GPa of phase I as shown in Figs. 5(a) and 5(b). Figures 5(c) and 5(d) show the closing of the gap at 13.5 GPa (phase II) and an increase of the DOS at the Fermi level at 37.8 GPa (phase III), respectively.

Partial densities of states from the angular momentum quantum number are given in Fig. 6. The PFY-XAS spectra of Se and Bi reflect the Se $4p$ DOS (peak A) and the weak Bi $6s$ DOS (peak D) and Bi $6d$ DOS (peaks E , F , and G), respectively, as described above. The broadening of the Se $4p$ band with pressure agrees with the experimental result in Fig. 3(b). The Se $4p$, Bi $6s$, and Bi $6d$ DOSs shift toward the Fermi level with pressure by changing the electronic structure, as shown in Fig. 6. Experimentally, although the Se- K absorption edge does not show a clear pressure dependence as shown in Fig. 3(c), the energy of the peak D in Fig. 3(i) and the Bi- L_3 absorption edge in Fig. 3(h) shift to lower energy, and both energies decrease suddenly around the pressure of the phase transition. Theoretically, the Bi $6s$ DOS just above the Fermi level increases with pressure as shown in Fig. 6, while the intensity of the Bi $6s$ band of the peak D decreases gradually above the pressure of the first phase transition experimentally, suggesting the decrease of the empty states of the Bi $6s$ band and the gradual increase of the carriers at high pressures. Both the theoretical and experimental results suggest that the emergence of the superconductivity strongly correlates to the

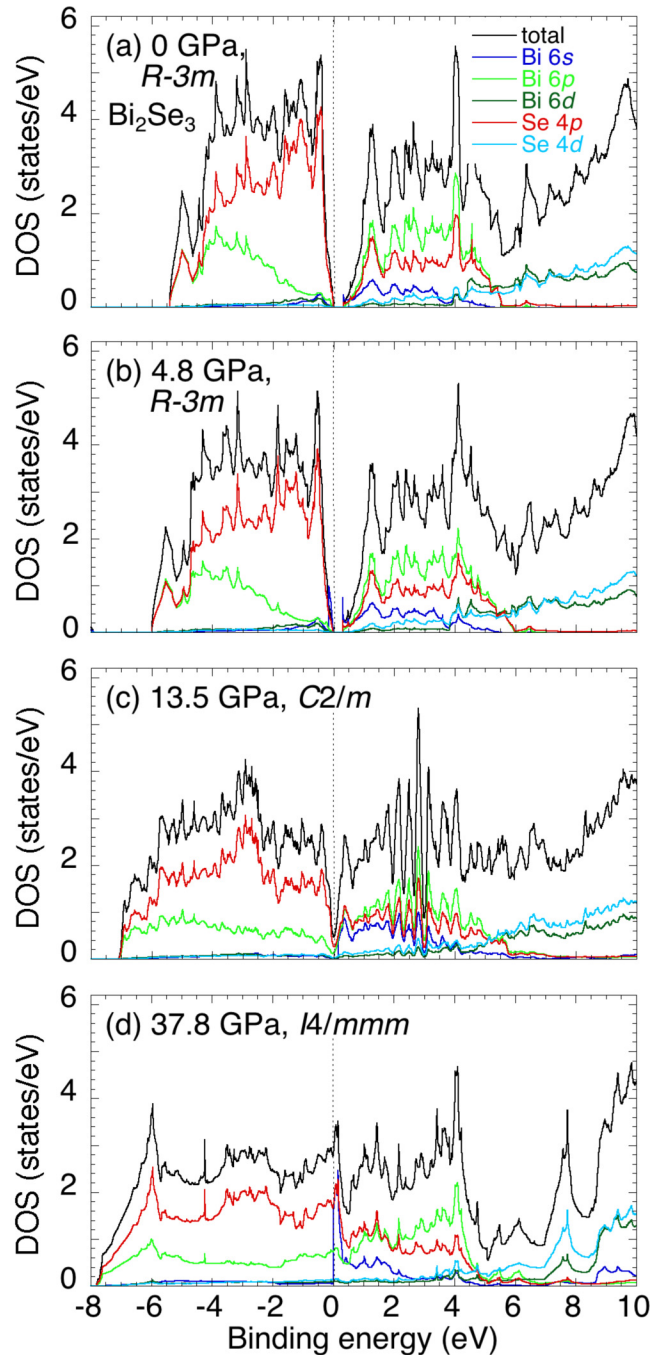


FIG. 6. Densities of states (DOS) of Bi_2Se_3 split by element and nl quantum numbers at four pressures, calculated with GGA+SO. Note that the DOS of Bi $6s$ at $E > E_F$ is multiplied by 30, where E is the binding energy.

closing of the band gap, where the DOS at the Fermi level increases abruptly, which may be triggered by the structural phase transition.

Figure 7 shows the pressure dependence of the band structures in the monoclinic phase II, where superconductivity was observed. We chose an in-plane k path with $L = (1/2, -1/2, 0)$, $X = (1/2, 0, 0)$, $Y = (0, 1/2, 0)$, and $M = (1/2, 1/2, 0)$. At 10 GPa, the valence-band maxima along the Γ - L direction cross the Fermi level, and the conduction-

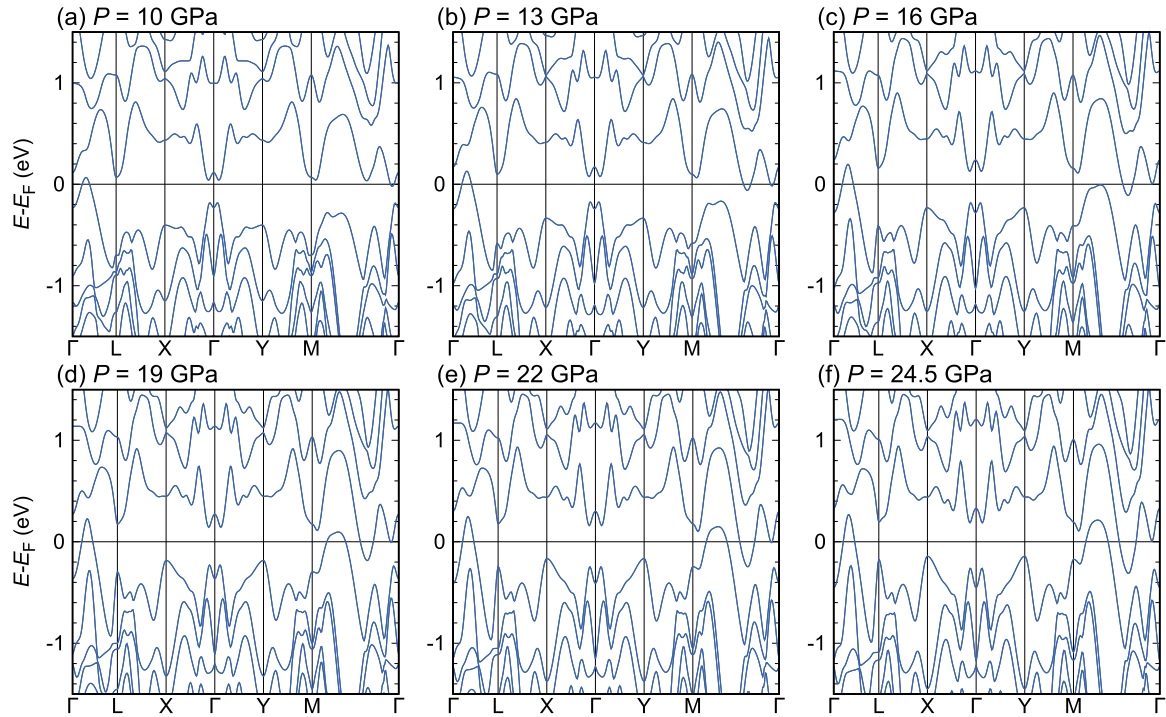


FIG. 7. Pressure dependence of the band structures in the monoclinic phase II. The crystal structures were taken from Ref. [39].

band minima along $M-\Gamma$ start to move down. At 16 GPa, the valence band along $M-\Gamma$ starts to cross the Fermi level, causing a small jump of the DOS at the Fermi level as shown in Fig. 8 below. These trends are emphasized with further increase of the pressure.

Total and partial s DOS as a function of pressure are shown in the Supplemental Material [44]. In phase I, the total DOS shifts to higher binding energy, keeping the band gap at the Fermi level. In phase II, the total DOS below the Fermi level shifts to higher binding energy, and above the Fermi level it shifts to lower binding energy. The DOS near the Fermi level increases, indicating the pressure-induced broadening of valence and conduction bands. In phase III, a similar trend to that in phase II was observed, but the DOS at the Fermi

level does not change much. Partial s DOS follows a similar trend to the total DOS in Fig. 6. A slight shift of the partial s DOS to higher binding energy with pressure corresponds to the gradual decrease of the peak D (Bi s DOS) energy in Fig. 3(i).

Figure 8 shows the pressure evolution of the DOS of Bi_2Se_3 at the Fermi level. The lattice parameters obtained from the literature were used and interpolated for the rhombohedral phase [71] and for the two monoclinic phases [39]. Calculations of the electronic structures at 88 pressure points were performed. In phase I, because of the band gap no DOS at the Fermi level was observed up to 10 GPa. The change in the DOS at the Fermi level is gradual in phase II and overall small, although the DOS appears abruptly at the beginning of phase II. There is a large change in the band structure between phases II and III, which originates from the upward shift of the valence bands as shown in Fig. 5(d) and simultaneously causes the sudden increase of the DOS at the Fermi level in Fig. 8. However, note that the two $C2/m$ phases have different unit cells, and thus it is difficult to compare the band structures. On the other hand, between phase II and phase III, Bi_2Se_3 experiences a 6% volume collapse. This leads to an increase of the effective coordination number of Bi. The concomitant rearrangement of states leads to a partial occupation of previously empty Bi $6p$ and Se $4p$ states [44]. These changes of the electronic structures cause the jump of the DOS at the Fermi level seen in Fig. 8. Meanwhile, the change in the electronic structure between phases II and III is small experimentally, as shown in Figs. 3 and 4. The experimental results are the integral intensity of the bands above the Fermi level, and thus they may be insensitive to the change in the DOS at the Fermi level. The calculated results clearly show the closing of the band gap around the 10 GPa of the first structural transition pressure. The carrier density increases by

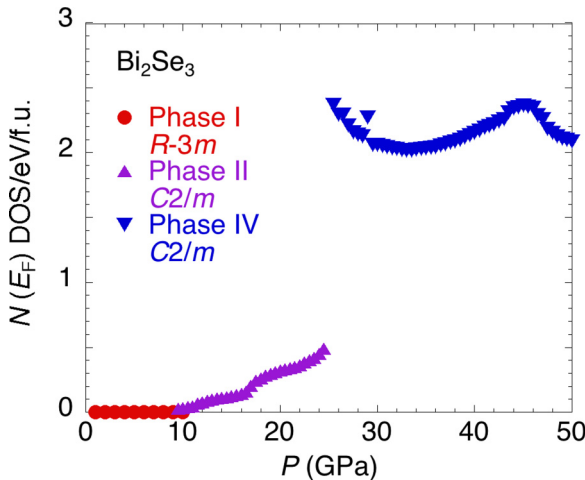


FIG. 8. Pressure evolution of the density of states at the Fermi level, based on the crystal structures from Ref. [39].

four orders of magnitude up to 47 GPa [5]. There is a small jump of the carrier density around the onset pressure of the superconductivity [5,7]. The present results of the DOS at the Fermi level show a strong correlation to the carrier density up to 25 GPa, but it does not change much in phase III and shows a rather similar trend to the pressure dependence of T_c [5], suggesting the promotion of T_c with the DOS at the Fermi level.

The Z_2 invariants for each crystal phase of Bi_2Se_3 under pressure were calculated, revealing a strong topological nature of $Z_2 = 1; (000)$ at 0 and 4.8 GPa (phase I), a topologically trivial nature of $Z_2 = 0; (000)$ at 13.5 GPa (phase II), and a strong topological nature of $Z_2 = 1; (111)$ at 37.8 GPa (phase III). Similar calculation results have been reported for $\text{Bi}_2\text{Te}_2\text{Se}$ [72]. Here, the topologically trivial nature at phase II as well as the topological state in the superconductivity phase are still under discussion because the Z_2 invariant in phase II is very sensitive to crystal structure.

The DFT calculations by other groups yielded similar results. Pseudopotential DFT calculations for Bi_2Se_3 by Gao *et al.* [73] showed Bi *s* DOS just above the Fermi level, which increases at 10 GPa compared to ambient pressure; the Fermi level shifts downward at 10 GPa. Cai *et al.* [60] suggested the loss of the nontrivial superconducting state in the monoclinic superconducting phase ($C2/m$, phase II) of $\text{Bi}_2\text{Te}_2\text{Se}$ by DFT calculations, taking into account the parities of each band. In the tetragonal superconducting phase ($I4/mmm$, phase III) there was no gap between the valence and conduction band without nontrivial topological character. This may suggest the absence of the topological nature in the superconducting phase under pressure. But further theoretical and experimental study may be required to understand the topological nature under pressure. A similar pressure-induced transition to the nontrivial Dirac semimetal state was also reported in $\text{Bi}_{1.5}\text{Sb}_{0.5}\text{Te}_{1.8}\text{Se}_{1.2}$ [61]. The DFT calculations showed that the bulk indirect band gap undergoes an indirect-to-direct band-gap transition at 5.8 GPa, the bulk band gap closes and develops a linear crossing of bands to form a 3D Dirac semimetal state at 8.24 GPa, and the system becomes a normal metal with further increase of the pressure before it undergoes the first structural phase transition to the metallic phases. These calculations showed a pressure-induced phase transition to the metallic state, closing of the gap, with the loss of the nontrivial state and with the emergence of the superconducting state. In contrast to the electronic structure under pressure, the scanning tunneling microscopy/spectroscopy at ambient pressure suggested the coexistence of the surface topological state with bulk superconductivity in $\text{Sr}_x\text{Bi}_2\text{Se}_3$ at ambient pressure, where DOS at the Fermi level was estimated to consist of <33% topological surface electrons and >67% normal bulk electrons [40].

Finally, we consider the spin-orbit coupling effect on the electronic structure. The GGA band gap (E_g) in Fig. 9(a) increases from 32 meV at 0 GPa to 56 meV at 4.8 GPa. On the other hand, the GGA+SO band gap in Fig. 9(b) decreases from 322 meV at 0 GPa to 296 meV at 4.8 GPa. We plot the evolution of the band gap up to 10 GPa based on the sequence of the band structures as shown in Fig. 9(c). The GGA band gap decreases up to 1 GP and increases gradually with further increase of the pressure while the GGA+SO gap shows an

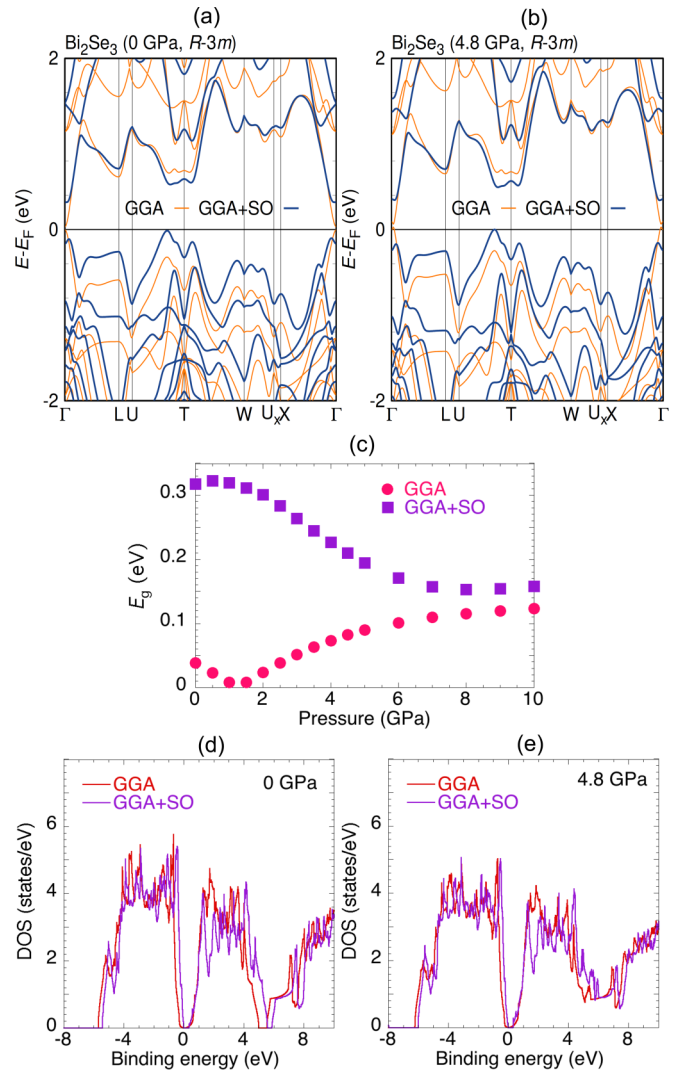


FIG. 9. Band structure of Bi_2Se_3 (a) at $P = 0$ and (b) $P = 4.8$ GPa, comparing GGA and GGA+SO calculations. A plot of the evolution of the band gap is shown in (c). Density of states (DOS) (d) at $P = 0$ and (e) $P = 4.8$ GPa is also shown.

opposite trend, but the difference of both gaps becomes small above 7 GPa. The spin-orbit coupling effect is also found as a decrease of DOS at an energy of approximately 1.7 eV above the Fermi level at low pressures, as shown in Fig. 9(d).

IV. CONCLUSIONS

We measured the pressure-induced changes in the electronic structure of the Bi_2Se_3 -based superconductors $\text{Ag}_{0.05}\text{Bi}_{1.95}\text{Se}_3$ and of the parent material Bi_2Se_3 . Pressure causes broadening of the bands such as the Se 4*p* DOS above the Fermi level and the shift of the Bi 6*s* band and the Bi- L_3 absorption energy to lower incident energies up to the pressure of the first structural transition.

In Bi_2Se_3 , a change in the Bi bulk electronic structure was observed around 4–5 GPa, where the pressure-induced electronic topological transition in the $R\bar{3}m$ phase has been suggested. In $\text{Ag}_{0.05}\text{Bi}_{1.95}\text{Se}_3$, the electronic structure changes

around the second phase transition pressure of 23 GPa and showed a trend to return to the structure below 8 GPa.

The DFT calculations of Bi₂Se₃ with fully relativistic GGA+SO showed the closing of the band gap around the pressure where the superconducting state emerged. The DFT calculations also show that the DOS at the Fermi level appears above the pressure of the first structural transition and is closely correlated with the pressure evolution of T_c .

These experimental and theoretical results may suggest a possible increase of the carrier density at the pressure of the first structural transition, which may correlate to the disappearance of the band gap, and the emergence of the superconductivity. The first structural phase transition is a trigger of the emergence of superconductivity where the electronic structure strongly changed, while above the pressure of the first phase transition the electronic structure does not change much and T_c may be kept nearly constant. These changes in the electronic structure may be common for the Bi₂Se₃ and the doped Bi₂Se₃ superconductors, although the shift of the phase transition pressure occurs by the doping.

The Z_2 invariants of Bi₂Se₃ showed the strong topological nature of $Z_2 = 1$ at phase I, a topologically trivial nature of $Z_2 = 0$ at phase II, and a strong topological nature of $Z_2 = 1$ at phase III. But it is noted that the Z_2 invariant in phase II is very sensitive to crystal structure.

In this study, we clarified the bulk electronic structure under pressure for the Bi₂Se₃-based compounds, and we showed the correlation with the first crystal structural transition and

the emergence of the superconductivity. To gain more insight into the behaviors of the electronic structure and the topological nature under pressure, further detailed investigation with the theoretical calculations will be desired.

ACKNOWLEDGMENTS

The experiments were performed at SPring-8 Taiwan beamline BL12XU (under SPring-8 Proposals No. 2018A4257, No. 2018B4251, No. 2019A4266, & No. 2019B4269 corresponding to NSRRC Proposals No. 2018-2-010, No. 2018-3-034, No. 2019-2-030, and No. 2019-3-004). Parts of the computations were carried out at the Supercomputer Center at the Institute for Solid State Physics, the University of Tokyo. Our deepest thanks go to Takaki Uchiyama and Akihisa Takai in Okayama University, and Yoshitaka Ueno and Yasunari Minami in Kwansai-Gakuin University for the help in the experiments. Ritsuko Eguchi in Okayama University kindly supported the sample preparation. We also appreciate the useful comments from Munetaka Taguchi about the pressure-induced change in the spectra, and from Keiichiro Imura in Nagoya University about the estimation of the carrier density in the Hall coefficient measurement. This work has been partly supported by Grants-in-Aid for Scientific Research (KAKENHI Grants No. 18K18736, No. 18K18743, and No. 19H02676) from MEXT and by the Program for Promoting the Enhancement of Research Universities.

-
- [1] H. Zhang, C.-X. Liu, X.-L. Qi, X. Dai, Z. Fang, and S.-C. Zhang, Topological insulators in Bi₂Se₃, Bi₂Te₃ and Sb₂Te₃ with a single Dirac cone on the surface, *Nat. Phys.* **5**, 438 (2009).
- [2] Y. L. Chen, J. G. Analytis, J.-H. Chu, Z. K. Liu, S.-K. Mo, X. L. Qi, H. J. Zhang, D. H. Lu, X. Dai, Z. Fang, S. C. Zhang, I. R. Fisher, Z. Hussain, and Z.-X. Shen, Experimental realization of a three-dimensional topological insulator Bi₂Te₃, *Science* **325**, 178 (2009).
- [3] M. Sato and Y. Ando, Topological superconductors: A review, *Rep. Prog. Phys.* **80**, 076501 (2017).
- [4] Y. Li and Z.-A. Xu, Exploring topological superconductivity in topological materials, *Adv. Quantum Technol.* **2**, 1800112 (2019).
- [5] K. Kirshenbaum, P. S. Syers, A. P. Hope, N. P. Butch, J. R. Jeffries, S. T. Weir, J. J. Hamlin, M. B. Maple, Y. K. Vohra, and J. Paglione, Pressure-Induced Unconventional Superconducting Phase in the Topological Insulator Bi₂Se₃, *Phys. Rev. Lett.* **111**, 087001 (2013).
- [6] H.-K. Mao, X.-J. Chen, Y. Ding, B. Li, and L. Wang, Solids, liquids, and gases under high pressure, *Rev. Mod. Phys.* **90**, 015007 (2018).
- [7] P. P. Kong, J. L. Zhang, S. J. Zhang, J. Zhu, Q. Q. Liu, R. C. Yu, Z. Fang, C. Q. Jin, W. G. Yang, X. H. Yu, J. L. Zhu, and Y. S. Zhao, Superconductivity of the topological insulator Bi₂Se₃ at high pressure, *J. Phys.: Condens. Matter* **25**, 362204 (2013).
- [8] Z. Yu, L. Wang, Q. Hu, J. Zhao, S. Yan, K. Yang, S. Sinogeikin, G. Gu, and H.-k. Mao, Structural phase transitions in Bi₂Se₃ under high pressure, *Sci. Rep.* **5**, 15939 (2015).
- [9] T. He, X. F. Yang, T. Terao, T. Uchiyama, T. Ueno, K. Kobayashi, J. Akimitsu, T. Miyazaki, T. Nishioka, K. Kimura, K. Hayashi, N. Hoppo, H. Yamaoka, H. Ishii, Y.-F. Liao, H. Ota, and Y. Kubozono, Pressure-induced superconductivity in Ag_xBi_{2-x}Se₃, *Phys. Rev. B* **97**, 104503 (2018).
- [10] A. M. Nikitin, Y. Pan, Y. K. Huang, T. Naka, and A. de Visser, High-pressure study of the basal-plane anisotropy of the upper critical field of the topological superconductor Sr_xBi₂Se₃, *Phys. Rev. B* **94**, 144516 (2016).
- [11] E. Uesugi, T. Uchiyama, H. Goto, H. Ota, T. Ueno, H. Fujiwara, K. Terashima, T. Yokoya, F. Matsui, J. Akimitsu, K. Kobayashi, and Y. Kubozono, Fermi level tuning of Ag-doped Bi₂Se₃ topological insulator, *Sci. Rep.* **9**, 5376 (2019).
- [12] T. V. Bay, T. Naka, Y. K. Huang, H. Luigjes, M. S. Golden, and A. de Visser, Superconductivity in the Doped Topological Insulator Cu_xBi₂Se₃ Under High Pressure, *Phys. Rev. Lett.* **108**, 057001 (2012).
- [13] Y. S. Hor, A. J. Williams, J. G. Checkelsky, P. Roushan, J. Seo, Q. Xu, H. W. Zandbergen, A. Yazdani, N. P. Ong, and R. J. Cava, Superconductivity in Cu_xBi₂Se₃ and its Implications for Pairing in the Undoped Topological Insulator, *Phys. Rev. Lett.* **104**, 057001 (2010).
- [14] K. Manikandan, Shruti, P. Neha, G. Kalai Selvan, B. Wang, Y. Uwatoko, K. Ishigaki, R. Jha, V. P. S. Awana, and S. Arumugam, Possibility for conventional superconductivity in Sr_{0.1}Bi₂Se₃ from high-pressure transport studies, *Europhys. Lett.* **118**, 47008 (2017).
- [15] Y. H. Zhou, X. L. Chen, R. R. Zhang, J. F. Shao, X. F. Wang, C. An, Y. Zhou, C. Y. Park, W. Tong, L. Pi, Z. R. Yang,

- C. J. Zhang, and Y. H. Zhang, Pressure-induced reemergence of superconductivity in topological insulator $\text{Sr}_{0.065}\text{Bi}_2\text{Se}_3$, *Phys. Rev. B* **93**, 144514 (2016).
- [16] Z. Liu, X. Yao, J. Shao, M. Zuo, L. Pi, S. Tan, C. Zhang, and Y. Zhang, Superconductivity with topological surface state in $\text{Sr}_x\text{Bi}_2\text{Se}_3$, *J. Am. Chem. Soc.* **137**, 10512 (2015).
- [17] L. Fu and E. Berg, Odd-Parity Topological Superconductors: Theory and Application to $\text{Cu}_x\text{Bi}_2\text{Se}_3$, *Phys. Rev. Lett.* **105**, 097001 (2010).
- [18] L. Fu, Odd-parity topological superconductor with nematic order: Application to $\text{Cu}_x\text{Bi}_2\text{Se}_3$, *Phys. Rev. B* **90**, 100509(R) (2014).
- [19] N. Levy, T. Zhang, J. Ha, F. Sharifi, A. A. Talin, Y. Kuk, and J. A. Stroscio, Experimental Evidence for s-wave Pairing Symmetry in Superconducting $\text{Cu}_x\text{Bi}_2\text{Se}_3$ Single Crystals Using a Scanning Tunneling Microscope, *Phys. Rev. Lett.* **110**, 117001 (2013).
- [20] C. Q. Han, H. Li, W. J. Chen, F. Zhu, M.-Y. Yao, Z. J. Li, M. Wang, B. F. Gao, D. D. Guan, C. Liu, C. L. Gao, D. Qian, and J.-F. Jia, Electronic structure of a superconducting topological insulator Sr-doped Bi_2Se_3 , *Appl. Phys. Lett.* **107**, 171602 (2015).
- [21] M. Neupane, Y. Ishida, R. Sankar, J.-X. Zhu, D. S. Sanchez, I. Belopolski, S.-Y. Xu, N. Alidoust, M. M. Hosen, S. Shin, F. Chou, M. Zahid Hasan, and T. Durakiewicz, Electronic structure and relaxation dynamics in a superconducting topological material, *Sci. Rep.* **6**, 22557 (2016).
- [22] K. Hämäläinen, D. P. Siddons, J. B. Hastings, and L. E. Berman, Elimination of the Inner-Shell Lifetime Broadening in X-Ray Absorption Spectroscopy, *Phys. Rev. Lett.* **67**, 2850 (1991).
- [23] K. Hämäläinen, C. C. Kao, J. B. Hasting, D. P. Siddons, L. E. Berman, V. Stojanoff, and S. P. Cramer, Spin-dependent x-ray absorption of MnO and MnF_2 , *Phys. Rev. B* **46**, 14274 (1992).
- [24] J.-P. Rueff and A. Shukla, Inelastic x-ray scattering by electronic excitations under high pressure, *Rev. Mod. Phys.* **82**, 847 (2010).
- [25] Z. Li, M. Wang, D. Zhang, N. Feng, W. Jiang, C. Han, W. Chen, M. Ye, C. Gao, J. Jia, J. Li, S. Qiao, D. Qian, B. Xu, H. Tian, and B. Gao, Possible structural origin of superconductivity in Sr-doped Bi_2Se_3 , *Phys. Rev. Mater.* **2**, 014201 (2018).
- [26] H. Yamaoka, Pressure dependence of the electronic structure of 4*f* and 3*d* electron systems studied by x-ray emission spectroscopy, *High Press. Res.* **36**, 262 (2016).
- [27] H. Yamaoka, Y. Yamamoto, E. F. Schwier, N. Tsujii, M. Yoshida, Y. Ohta, H. Sakurai, J.-F. Lin, N. Hiraoka, H. Ishii, K.-D. Tsuei, M. Arita, K. Shimada, and J. Mizuki, Pressure-induced phase transition in LaCo_5 studied by x-ray emission spectroscopy, x-ray diffraction and density functional theory, *Phys. Rev. B* **94**, 165156 (2016).
- [28] H. Yamaoka, Y. Yamamoto, J.-F. Lin, Junjie J. Wu, X. Wang, C. Jin, M. Yoshida, S. Onari, S. Ishida, Y. Tsuchiya, N. Takeshita, N. Hiraoka, H. Ishii, K.-D. Tsuei, P. Chow, Y. Xiao, and J. Mizuki, Electronic structures and spin states of BaFe_2As_2 and SrFe_2As_2 probed by x-ray emission spectroscopy at Fe and As K-absorption edges, *Phys. Rev. B* **96**, 085129 (2017).
- [29] H.-K. Mao and P. M. Bell, High-pressure physics: The 1-megabar mark on the ruby *R1* static pressure scale, *Science* **191**, 851 (1976).
- [30] K. Syassen, Ruby under pressure, *High Press. Res.* **28**, 75 (2008).
- [31] H. Yamaoka, Y. Zekko, I. Jarrige, J.-F. Lin, N. Hiraoka, H. Ishii, K.-D. Tsuei, and J. Mizuki, Ruby pressure scale in a low-temperature diamond anvil cell, *J. Appl. Phys.* **112**, 124503 (2012).
- [32] X. Chen, H. D. Zhou, A. Kiswandhi, I. Miotkowski, Y. P. Chen, P. A. Sharma, A. L. Lima Sharma, M. A. Hekmaty, D. Smirnov, and Z. Jiang, Thermal expansion coefficients of Bi_2Se_3 and Sb_2Te_3 crystals from 10 K to 270 K, *Appl. Phys. Lett.* **99**, 261912 (2011).
- [33] K. Koepf and H. Eschrig, Full-potential nonorthogonal local-orbital minimum-basis band-structure scheme, *Phys. Rev. B* **59**, 1743 (1999).
- [34] J. P. Perdew, K. Burke, and M. Ernzerhof, Generalized Gradient Approximation Made Simple, *Phys. Rev. Lett.* **77**, 3865 (1996).
- [35] T. Uchiyama, H. Goto, E. Uesugi, A. Takai, L. Zhi, S. Hamao, R. Eguchi, H. Ota, K. Sugimoto, A. Fujiwara, F. Matsui, K. Kimura, K. Hayashi, T. Ueno, K. Kobayashi, J. Akimitsu, and Y. Kubozono, Fermi-level pinning in Bi_2Se_3 due to impurity doping (unpublished).
- [36] F. Matsui *et al.* (unpublished).
- [37] R. Vilaplana, D. Santamaría-Pérez, O. Gomis, F. J. Manjón, J. González, A. Segura, A. Muñoz, P. Rodríguez-Hernández, E. Pérez-González, V. Marín-Borrás, V. Muñoz-Sanjose, C. Drasar, and V. Kucek, Structural and vibrational study of Bi_2Se_3 under high pressure, *Phys. Rev. B* **84**, 184110 (2011).
- [38] J. Zhao, H. Liu, L. Ehm, D. Dong, Z. Chen, and G. Gu, High-pressure phase transitions, amorphization, and crystallization behaviors in Bi_2Se_3 , *J. Phys.: Condens. Matter* **25**, 125602 (2013).
- [39] G. Liu, L. Zhu, Y. Ma, C. Lin J. Liu, and Y. Ma, Stabilization of 9/10-fold structure in bismuth selenide at high pressures, *J. Phys. Chem. C* **117**, 10045 (2013).
- [40] G. Du, J. Shao, X. Yang, Z. Du, D. Fang, J. Wang, K. Ran, J. Wen, C. Zhang, H. Yang, Y. Zhang, and H.-H. Wen, Drive the Dirac electrons into Cooper pairs in $\text{Sr}_x\text{Bi}_2\text{Se}_3$, *Nat. Commun.* **8**, 14466 (2017).
- [41] A. N. Baranov, J. S. Kim, D. C. Kim, D. S. Suh, Y. W. Park, and E. V. Antipov, X-ray absorption near-edge structure spectra study of the $\text{Ba}_{1-x}\text{K}_x\text{BiO}_3$ ($0.37 \leq x \leq 1.0$) superconductor, *Physica C* **383**, 95 (2002).
- [42] Q. Zhou, P. E. R. Blanchard, B. J. Kennedy, C. D. Ling, S. Liu, M. Avdeev, J. B. Aitken, A. Tadich, and H. E. A. Brand, Diffraction and spectroscopic study of pyrochlores $\text{Bi}_{2-x}\text{Fe}_{1+x}\text{SbO}_7$, *J. Alloys Compd.* **589**, 425 (2014).
- [43] J. Deng and Z.-Y. Zhao, Electronic structure and optical properties of bismuth chalcogenides Bi_2Q_3 ($Q = \text{O}, \text{S}, \text{Se}, \text{Te}$) by first-principles calculations, *Comput. Mater. Sci.* **142**, 312 (2018).
- [44] See Supplemental Material at <http://link.aps.org/supplemental/10.1103/PhysRevB.102.155118>, which includes Refs. [10,14–16,25,63,64,70]. Pressure dependence of the electronic structure of $\text{Sr}_x\text{Bi}_2\text{Se}_3$ and Bi, and additional calculation results are shown.
- [45] B. Joseph, A. Iadecola, L. Simonelli, Y. Mizuguchi, Y. Takano, T. Mizokawa, and N. L. Saini, A study of the electronic structure of $\text{FeSe}_{1-x}\text{Te}_x$ chalcogenides by Fe and Se *K*-edge x-ray absorption near edge structure measurements, *J. Phys.: Condens. Matter* **22**, 485702 (2010).

- [46] C. L. Chen, S. M. Rao, C. L. Dong, J. L. Chen, T. W. Huang, B. H. Mok, M. C. Ling, W. C. Wang, C. L. Chang, and T. S. Chan, X-ray absorption spectroscopy investigation of the electronic structure of superconducting FeSe_x single crystals, *Europhys. Lett.* **93**, 47003 (2011).
- [47] N. L. Saini, T. Mizokawa, E. Magnano, S. Nappini, F. Bondino, H. Takeya, Y. Mizuguchi, Y. Takano, and K. B. Garg, X-ray absorption and photoemission spectroscopy of electronic phase separation in K_xFe_{2-y}Se₂, *Phys. Rev. B* **90**, 184510 (2014).
- [48] A. I. Figueroa, G. der Laan, L. J. Collins-McIntyre, G. Cibin, A. J. Dent, and T. Hesjedal, Local structure and bonding of transition metal dopants in Bi₂Se₃ topological insulator thin films, *J. Phys. Chem. C* **119**, 17344 (2015).
- [49] A. A. Rahman, R. Huang, and L. Whittaker-Brooks, Distinctive extrinsic atom effects on the structural, optical, and electronic properties of Bi₂S_{3-x}Se_x solid solutions, *Chem. Mater.* **28**, 6544 (2016).
- [50] N. Jiang and J. C. H. Spence, Can near-edge structure of the Bi L₃ edge determine the formal valence states of Bi? *J. Phys.: Condens. Matter* **18**, 8029 (2006).
- [51] S. M. Heald, D. DiMarzio, M. Croft, M. S. Hegde, S. Li, and M. Greenblatt, X-ray-absorption study of charge-density ordering in (Ba_{1-x}K_x)BiO₃, *Phys. Rev. B* **40**, 8828 (1989).
- [52] R. Retoux, F. Studer, C. Michel, B. Raveau, A. Fontaine, and E. Dartige, Valence state for bismuth in the superconducting bismuth cuprates, *Phys. Rev. B* **41**, 193 (1990).
- [53] P. P. Kong, F. Sun, L. Y. Xing, J. Zhu, S. J. Zhang, W. M. Li, Q. Q. Liu, X. C. Wang, S. M. Feng, X. H. Yu, J. L. Zhu, R. C. Yu, W. G. Yang, G. Y. Shen, Y. S. Zhao, R. Ahuja, H. K. Mao, and C. Q. Jin, Superconductivity in strong spin orbital coupling compound Sb₂Se₃, *Sci. Rep.* **4**, 6679 (2014).
- [54] J. Zhu, J. L. Zhang, P. P. Kong, S. J. Zhang, X. H. Yu, J. L. Zhu, Q. Q. Liu, X. Li, R. C. Yu, R. Ahuja, W. G. Yang, G. Y. Shen, H. K. Mao, H. M. Weng, X. Dai, Z. Fang, Y. S. Zhao, and C. Q. Jin, Superconductivity in topological insulator Sb₂Te₃ induced by pressure, *Sci. Rep.* **3**, 2016 (2013).
- [55] M. L. Jin, F. Sun, L. Y. Xing, S. J. Zhang, S. M. Feng, P. P. Kong, W. M. Li, X. C. Wang, J. L. Zhu, Y. W. Long, H. Y. Bai, C. Z. Gu, R. C. Yu, W. G. Yang, G. Y. Shen, Y. S. Zhao, H. K. Mao, and C. Q. Jin, Superconductivity bordering Rashba type topological transition, *Sci. Rep.* **7**, 39699 (2013).
- [56] J. R. Jeffries, N. P. Butch, Y. K. Vohra, and S. T. Weir, Pressure evolution of electrical transport in the 3D topological insulator (Bi, Sb)₂(Se, Te)₃, *J. Phys.: Conf. Ser.* **592**, 012124 (2015).
- [57] C. An, X. Chen, B. Wu, Y. H. Zhou, Y. Zhou, R. Zhang, C. Park, F. Song, and Z. Yang, Pressure-induced topological insulator-to-metal transition and superconductivity in Sn-doped Bi_{1.1}Sb_{0.9}Te₂S, *Phys. Rev. B* **97**, 174516 (2018).
- [58] A. Gaul, Q. Peng, D. J. Singh, G. Ramanath, and T. Borca-Tasciuc, Pressure-induced insulator-to-metal transitions for enhancing thermoelectric power factor in bismuth telluride-based alloys, *Phys. Chem. Chem. Phys.* **19**, 12784 (2017).
- [59] A. Bera, K. Pal, D. V. S. Muthu, U. V. Waghmare, and A. K. Sood, Pressure-induced phase transition in Bi₂Se₃ at 3 GPa: electronic topological transition or not? *J. Phys.: Condens. Matter* **28**, 105401 (2016).
- [60] S. Cai, S. K. Kushwaha, J. Guo, V. A. Sidorov, C. Le, Y. Zhou, H. Wang, G. Lin, X. Li, Y. Li, K. Yang, A. Li, Q. Wu, J. Hu, R. J. Cava, and L. Sun, Universal superconductivity phase diagram for pressurized tetradymite topological insulators, *Phys. Rev. Mater.* **2**, 114203 (2018).
- [61] J.-S. Kim, R. Juneja, N. P. Salke, W. Palosz, V. Swaminathan, S. Trivedi, A. K. Singh, D. Akinwande, and J.-F. Lin, Structural, vibrational, and electronic topological transitions of Bi_{1.5}Sb_{0.5}Te_{1.8}Se_{1.2} under pressure, *J. Appl. Phys.* **123**, 115903 (2019).
- [62] M. P. Smylie, K. Willa, K. Ryan, H. Claus, W.-K. Kwok, Y. Qiu, Y. S. Hor, and U. Welp, An increase in T_c under hydrostatic pressure in the superconducting doped topological insulator Nb_{0.25}Bi₂Se₃, *Physica C* **543**, 58 (2017).
- [63] H. Leng, D. Cherian, Y. K. Huang, J.-C. Orain, A. Amato, and A. de Visser, Muon spin rotation study of the topological superconductor Sr_xBi₂Se₃, *Phys. Rev. B* **97**, 054503 (2018).
- [64] H.-Y. Chen, S.-K. Xiang, X.-Z. Yan, L.-R. Zheng, Y. Zhang, S.-G. Liu, and Y. Bi, Phase transition of solid bismuth under high pressure, *Chin. Phys.* **25**, 108103 (2016).
- [65] Z. Guo, H. Zhu, J. Dong, Q. Jia, Y. Gong, Y. Wang, H. Li, P. An, D. Yang, Y. Zhao, H. Xing, X. Li, and D. Chen, Local structural changes during the disordered substitutional alloy transition in Bi₂Te₃ by high-pressure XAFS, *J. Appl. Phys.* **124**, 065901 (2018).
- [66] M. A. Il'ina and E. S. Itskevich, New superconducting modifications of Bismuth, *JETP Lett.* **11**, 218 (1972).
- [67] M. A. Il'ina, Superconducting properties of the bismuth-antimony system at high pressures, *Sov. Phys. Solid State* **18**, 600 (1976).
- [68] C. G. Homan, Phase diagram of Bi up to 140 kbars, *J. Phys. Chem. Solids* **36**, 1249 (1975).
- [69] M. I. McMahon, O. Degtyareva, and R. J. Nelmes, Ba-IV-Type Incommensurate Crystal Structure in Group-V Metals, *Phys. Rev. Lett.* **85**, 4896 (2000).
- [70] Y. Li, E. Wang, X. Zhu, and H.-H. Wen, Pressure-induced superconductivity in Bi single crystals, *Phys. Rev. B* **95**, 024510 (2017).
- [71] H. Cheng, J. Zhang, Y. Li, G. Li, and X. Li, Structure determination of the high-pressure phases of topological insulator Bi₂Se₃ using experiments and calculations, *J. Appl. Phys.* **121**, 225902 (2017).
- [72] T. He, X. Yang, T. Taguchi, T. Ueno, K. Kobayashi, J. Akimitsu, H. Yamaoka, H. Ishii, Y.-F. Liao, H. Ota, H. Goto, R. Eguchi, K. Terashima, T. Yokoya, H. O. Jeschke, X. Wu, and Y. Kubozono, Pressure-induced superconductivity in Bi_{2-x}Sb_xTe_{3-y}Se_y, *Phys. Rev. B* **100**, 094525 (2019).
- [73] X. Gao, M. Zhou, Y. Cheng, and G. Ji, First-principles study of structural, elastic, electronic and thermodynamic properties of topological insulator Bi₂Se₃ under pressure, *Philos. Mag.* **96**, 208 (2016).